Strong bonding between sputtered bioglass-ceramic films and Ti-substrate implants induced by atomic inter-diffusion post-deposition heat-treatments

ARTICLE *in* APPLIED SURFACE SCIENCE · SEPTEMBER 2013

Impact Factor: 2.71 · DOI: 10.1016/j.apsusc.2013.05.022

Applied Surface Science 280 (2013) 530–538

Contents lists available at SciVerse ScienceDirect

Applied Surface Science

journal homepage: www.elsevier.com/locate/apsusc

Strong bonding between sputtered bioglass–ceramic films and Ti-substrate implants induced by atomic inter-diffusion post-deposition heat-treatments

G.E. Stan[a,*], A.C. Popa[a,b,c], A.C. Galca[a], G. Aldica[a], J.M.F. Ferreira[d]

[a] National Institute of Materials Physics, Bucharest-Magurele 077125, Romania
[b] Army Centre for Medical Research, Bucharest 020012, Romania
[c] Department of Cellular and Molecular Medicine, "Carol Davila" University of Medicine and Pharmacy, Bucharest 050474, Romania
[d] Department of Materials and Ceramics Engineering, CICECO, University of Aveiro, Aveiro 3810-193, Portugal

ARTICLE INFO

Article history:
Received 1 March 2013
Received in revised form 1 May 2013
Accepted 6 May 2013
Available online 13 May 2013

Keywords:
Glass–ceramic thin films
Magnetron sputtering
Heat-treatment
Inter-diffusion phenomena
XRD
Pull-out adherence

ABSTRACT

Bioglasses (BG) are the inorganic materials exhibiting the highest indices of bioactivity. Their appliance as films for bio-functionalization of metallic implant surfaces has been regarded as an optimal solution for surpassing their limited bulk mechanical properties. This study reports on magnetron sputtering of alkali-free BG thin films by varying the target-to-substrate working distance, which proved to play an important role in determining the films' properties. Post deposition heat-treatments at temperatures slightly above the glass transformation temperature were then applied to induce inter-diffusion processes at the BG/titanium substrate interface and strengthening the bonding as determined by pull-out adherence measurements. The morphological and structural features assessed by SEM–EDS, XRD, and FTIR revealed a good correlation between the formations of inter-metallic titanium silicide phases and the films' bonding strength. The highest mean value of pull-out adherence (60.3 ± 4.6 MPa), which is adequate even for load-bearing biomedical applications, was recorded for films deposited at a working distance of 35 mm followed by a heat-treatment at 750 °C for 2 h in air. The experimental findings are explained on the basis of structural, compositional and thermodynamic considerations.

1. Introduction

Bioactive ceramics and glasses have been on the focus for decades [1,2] due to their capability of enhancing the repair of conjunctive hard tissues. Since the beginning of the 1990s the endo-prostheses and implants coated with such type of materials have been regarded as the next improved generation of medical devices. The stepping stone for achieving a successful implant-type coating design is given by the fulfillment of two ineluctable requirements: excellent biocompatibility and reliable mechanical properties.

For hydroxyapatite [$Ca_{10}(PO_4)_6(OH)_2$], the foremost exponent of the bioactive ceramics family, successful coating procedures/designs for medical implants have been found [3]. Bioactive glasses (BG) are osteoproductive-type inorganic materials, eliciting both intracellular and extracellular interface responses and possessing the best bioactive output in terms of rate of interfacial bonding with the host (hard or soft) tissues. They also activate genes that stimulate regeneration of living tissues by ionic exchange, opening the way for third generation implants [1,4]. However, no significant technological progresses toward obtaining safe and reliable BG coatings on metallic substrates were made so far.

The limited interfacial mechanical properties are the major factor hindering the use of BG/Ti structures for load-bearing applications [5–8]. The mismatch between the coefficients of thermal expansion of BG coatings [$(11–17) \times 10^{-6}\,°C^{-1}$] [2], and medical-grade Ti substrates ($\sim 9.2 \times 10^{-6}\,°C^{-1}$) is the main factor responsible for the limiting interfacial bonding strength of BG/Ti joint and for its susceptibility to micro-cracking and delamination.

The increasing demand for high-quality long-term sustainable implants led to a frantic search for new materials, technologies and architectural concepts, and thus the interest in biocompatible coatings and thin films increased exponentially [2,5,9]. Subsequently, important progresses have been made in the bioactive glass powder preparation [2,10], as well as in the glass and glass–ceramic coatings' processing [2,5]. Obtaining high performance thin bioactive glass films was attempted by using a variety of coating methods including wet sol–gel technology [7], electrophoretic deposition [11], enameling [12,13], plasma spraying [6], high-velocity suspension flame spraying [14], suspension

* Corresponding author. Tel.: +40 724131131; fax: +40 213690177.
E-mail addresses: george_stan@infim.ro, george_stan@ymail.com (G.E. Stan).

0169-4332/$ – see front matter © 2013 Elsevier B.V. All rights reserved.
http://dx.doi.org/10.1016/j.apsusc.2013.05.022

plasma spraying [15], pulsed laser deposition (PLD) [16], and radio-frequency magnetron sputtering (RF-MS) [9,17].

Unlike many of the competitor deposition techniques, RF-MS allows the synthesis of uniform films over large area substrates even having complex 3D geometries [18]. It also allows an easy and efficient technological transfer to industry as proved in the past for decorative and semiconductor manufacturing. High purity RF-MS films with densities close to bulk (target) materials and reasonable mechanical properties have been reported [9,18]. But their low interfacial substrate/coating adherence still remains as major problem [2,6–8], and several architectural designs have been proposed recently to overcome it. The attempts made include the intercalation of adhesion buffer layers, simple or with compositional gradients Ti_xBG_{1-x} (x = 0–1) [12,13,19,20], the reinforcement of glass structures with various compounds [21,22], and tailoring the glass chemical composition [2,23]. For example, alkali-free bioglass depicting excellent bioactivity and good sintering ability were recently disclosed [24] to overcome the drawbacks of incorporating alkali cations that were proved to induce a few setbacks: (i) enhanced coefficient of thermal expansion; (ii) increased tendency for crystallization; (iii) higher susceptibility for water uptake by osmosis resulting in *in vivo* instability [19,24].

To avoid the above mentioned problems, an alkali-free glass composition (wt.%: SiO_2 – 30, CaO – 28.6, P_2O_5 – 24.15, MgO – 17.25), with excellent *in vitro* bioactivity [8,25], was chosen as target material and two fixed target-to-substrate distances were selected for the RF-MS deposition of the thin films object of the present study. The aim is to further apply post-deposition thermal treatments and systematically studying the effects of processing parameters on the interfacial BG/Ti bonding by inducing the formation of an inter-diffusion Ti–Si mix phase. Identifying the strengthening mechanisms and selecting the most suitable processing conditions for increasing the BG/Ti adherence will favor predictability of properties instead of serendipity.

2. Materials and methods

2.1. BG powder synthesis. Cathode target preparation

Reagent grade powders of SiO_2 (Sigma–Aldrich, purity ≥ 99.8%), $Ca(H_2PO_4)_2{\cdot}H_2O$ (Loba Chemie, purity ≥ 95%), $CaCO_3$ (Sigma–Aldrich, purity ≥ 99.9%), and MgO (Sigma–Aldrich, purity ≥ 99.9%) were used for preparing the bioglass. Homogeneous mixtures of batches (~150 g) obtained by ball milling in ethanol were dried 6 h and then calcined using heating ramps of 5 °C min^{-1} up to 750 °C, a slower heating rate (2 °C min^{-1} up to 1000 °C), followed by a holding time of 12 h at this temperature for complete decarbonization and then melted in a Pt crucible in air at 1500 °C for 2 h. A glass frit was obtained by quenching the melt into cold water followed by drying and milling in a high-speed porcelain mill to obtain a fine powder with a mean particle size of (~20–25 μm) measured by light scattering technique (Malvern Mastersizer 3000, Mie-Fraunhofer model).

The magnetron cathode BG targets (110 mm diameter, 3 mm thick) were manufactured by mild-pressing the as-prepared glass powder into titanium dishes at room temperature, a time and cost efficient approach with proven consistency for sputtering process [17,26] that avoids targets' breakage.

2.2. Deposition procedure

High purity (99.6%) commercial titanium (Ti) (Mateck GmbH), a common material used in dentistry implantology, was selected as substrate in form of 15 mm × 15 mm plate squares with 1 mm thickness. The Ti specimens were polished with SiC papers of decreasing grain sizes down to grit 1200. Parallel depositions were also made on silicon wafers (1 0 0) to enable estimating the films' thickness by spectroscopic ellipsometry. Before deposition, all the substrates were previously cleaned *ex situ* by successive ultrasonic washing for 10 min in acetone and ethanol, followed by drying in nitrogen flow, and by *in situ* plasma etching in argon atmosphere for around 10 min.

A UVN-75-R1 sputtering deposition system having a magnetron cathode with a plasma ring of ~55 mm diameter was used to deposit the BG thin films. Spectral argon was admitted up to 0.4 Pa (the sputtering pressure) into the sputtering chamber that has been firstly evacuated to a pressure $<3 \times 10^{-3}$ Pa. A constant total gas flow rate of 45 standard cubic centimeters per minute was kept for all depositions. The radio-frequency generator (1.78 MHz) was maintained at a constant and low RF power (~100 W) to avoid the parching of the target surface which could produce undesirable radiative heating effects on the substrates and growing films.

The sputtering of BG thin films was carried out for 1 h, using two target-to-substrate distances (D_{T-S}): 35 mm (sample code BGa) and 55 mm (sample code BGb). During deposition the target surface reached a temperature of ~350 °C, while the substrates had a temperature close to ~150 °C at D_{T-S} = 35 mm and of ~120 °C at D_{T-S} = 55 mm, as estimated with a built-in temperature controller. The substrates and growing films' temperature was dependent on plasma self-heating. On the basis of the differential thermal analysis for the powder target, post-deposition heat-treatments (PDHT) in air at 750 °C for 2 h have been performed for a series of BG samples.

2.3. Characterization of sputtered glass-based thin films

Differential thermal analysis (SETARAM Setsys Evolution 18) experiments were conducted in the Thermal Analyzer TG-DSC mode within the temperature range of 30–1000 °C to characterize the thermal behavior of the bioglass powder. The experiments were conducted in synthetic air (80% N_2/20% O_2, 5 N) at a flow rate of 16 mL min^{-1} using approximately the same weight (46.3 ± 4.5 mg) of glass powder. The temperature was calibrated with bismuth, aluminum and silver. Nominal heating rates of 4, 5 and 30 °C min^{-1} were used and the temperature and the sample weight were continuously recorded. DTA diagrams were used to estimate the glass transition temperature (T_g) and the crystallization temperatures (T_c) at which the phases' crystallization occur. Values of T_g^{onset} and T_g^{offset} were determined from the intersection points of curve tangents. The reported results are the average values of the two measurements, with an experimental error of ±2 °C.

The optical measurements were done with a Woollam Variable Angle Spectroscopic Ellipsometer (VASE) system, equipped with a high pressure Xe discharge lamp incorporated in an HS-190 monochromator. Measurements were performed in the IR–Vis–UV region of the spectrum at energies between 1 and 6.2 eV, step of 0.01 eV, at 45°, 60° and 75° angles of incidence.

The morphology of the films was examined by scanning electron microscopy (SEM), using an Hitachi S2600N apparatus (20 kV acceleration voltage and 10 μA beam current) under secondary electron mode. Energy dispersive X-ray (EDX) spectroscopy (Edwin WinTools instrument) was used to estimate the local chemical compositions of the areas under analysis. The experimental reproducibility of EDX measurements was check for by analyzing five different regions of 20 μm × 20 μm for each sample. A statistical estimation – mean ± standard deviation (SD) – was obtained based on the recorded values.

A Bruker D8 Advance diffractometer in the powder setting mode with Cu K_α (λ = 1.5418 Å) radiation was used to identify the crystalline phases. The scattered intensity was scanned in the range 20–50° (2θ), with a step size of 0.04°. The diffractometer was

equipped with a high efficiency one-dimensional detector (Lynx Eye type) operated in integration mode. Samples were spin at 30 rpm during overnight data collection in order to average over possible inhomogeneities of the surface layer and because of the very low intensity scattered radiation.

Fourier Transform Infrared (FTIR) spectroscopic analyses were carried out for the detection of the functional groups present in the BG target and films, using a Perkin Elmer BX Spectrum-Pike spectrometer in Attenuated Total Reflection (ATR, Pike-MIRacle diamond head) mode. The spectra were collected over 550–1800 cm^{-1} range, by recording 150 individual scans at 4 cm^{-1} resolution.

The pull-out measurements were carried out using a DFD Instruments PAT MICRO adhesion tester AT101 (maximum pull force = 1 kN) equipped with Φ 2.8 mm stainless steel test elements. The experimental procedure was conducted in accordance with the ASTM D4541-09e1 standard. The test elements were glued to the film's surface with an E1100S cyanoacrylate epoxy adhesive. The stub surface was firstly polished, ultrasonically degreased in acetone and ethanol and dried in a nitrogen flow. After gluing, the samples were placed in an oven for thermal curing (130 °C for 1 h). Each test element was pulled-out vertically with a calibrated hydraulic pump until detachment. The adhesion strength was determined from the recorded failure value divided by the quantified detached surface area. For each type of sample, 5 individual assays were conducted. Mean values and standard deviations (SD) were computed. The statistical significance was determined using an unpaired Student's *t*-test. The differences were considered significant when $p < 0.05$.

3. Results

3.1. DTA results

Fig. 1 presents the DTA in DSC mode curves of the bioglass at three heating rates. The endothermic effect was assigned to the glass transition temperature T_g. There are three different points on the heat flow *versus* temperature curves that can be used to determine T_g: the onset (T_g^{onset}), middle, and offset (T_g^{offset}) transition temperatures. Only the middle values are presented in Fig. 1. Glass crystallization temperatures (T_c) are also depicted in Fig. 1. The peak positions shifted to higher temperatures and the peaks became broader with increasing heating rate.

Based on these results, the following post-deposition heat-treatment conditions were selected: a maximum temperature of 750 °C (slightly higher than T_g), heating and cooling rates of 5 °C min^{-1}, slow enough to minimize residual mechanical stresses in films at the end of the thermal cycle.

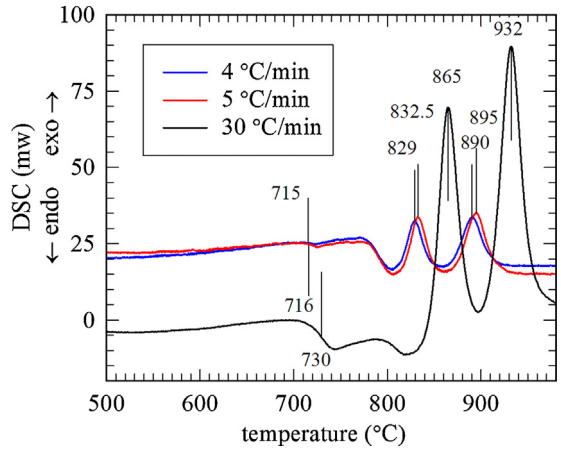

Fig. 1. DSC diagram recorded at different heating rates, in synthetic air.

3.2. Spectroscopic ellipsometry results

Films of small thickness were deliberately chosen to facilitate the inter-diffusion studies. The thickness values for the as-deposited BG/Si films measured by spectroscopic ellipsometry using the model proposed elsewhere [27] were as follows: 445 ± 3 nm for BGa (D_{T-S} = 35 mm), and 364 ± 3 nm for BGb (D_{T-S} = 55 mm). Two complementary physical processes account for the decreasing deposition rate with increasing the target-to-substrate distance (while keeping constant other sputtering parameters): (i) the angular emission type from the target; (ii) the gas phase scattering. The relevance of gas phase scattering can be neglected in the present deposition conditions, as the mean free path of sputtered atoms is larger than any of the D_{T-S} used [28,29]. Therefore, the cosine-like angular distribution from the target is the main factor responsible for the observed deposition rate decay. At longer D_{T-S}, more atoms emitted at larger angles are likely to collide with the reactor walls instead of reaching the substrate.

3.3. SEM–EDX analyses

Fig. 2 displays the SEM images collected in secondary electrons mode for the BG films as-deposited and after the post-deposition heat-treatment (PDHT) at 750 °C for 2 h in air. A smooth morphology can be observed for the as-deposited BG thin films, irrespective of the target-to-substrate distance used, consisting of fine rounded formations of quasi-uniform dimensions. This smooth morphology, a typical feature of amorphous layers deposited by RF-MS [30], acquired an obvious rougher granular appearance after PDHT. The SEM micrographs reveal that large clusters of grains with relatively well-defined boundaries and dimensions in range of 150–300 nm were formed at the films' surface as a result of devitrification. These granular features being more evident in the BGb films, suggest that a more extended devitrification process has occurred for the film deposited at the longer D_{T-S}. The more severe loss of some atoms (that did not reach the target) and the smaller thickness of BGb films might be the undelaying reasons for the morphological differences observed [31]. The general topography of annealed films is homogeneous and free from micro-cracks, gas bubbles and delaminations. An increased surface roughness of a coated implant can improve the intra-tissular retention (thus avoiding micro-movements *in situ*) and increase the contact surface area (determining the extent of cell colonization) [32].

The oxides composition (mean ± SD) for the as-deposited samples and the powder target, determined on the basis of EDX data, are plotted comparatively in Fig. 3. Even considering the well-known low accuracy (<5 at.%) of EDX quantitative analysis, the regular behavior of experimental data enables drawing some conclusions: (i) the target composition is not stoichiometrically transferred to the films; (ii) the films became significantly enriched in MgO and proportionally depleted in CaO, while their SiO_2 and P_2O_5 contents are similar to those in parent target. Based on these results, it seems reasonable to hypothesize that the atomic mass, the bond strength and the affinity of the different glass elements toward oxygen are likely to affect the sputtering transfer, and thus will determine the films' composition. Similar, but not identical trends have been observed in previous studies when using different glass compositions [17], suggesting that the atomic mass transfer is likely to be affected by the specific bioglass composition. Considering the closeness of the standard free energies for oxidation of Mg and Ca (Table 1), the enrichment of the films in MgO and the concomitant depletion in CaO suggest that atomic weight might be playing

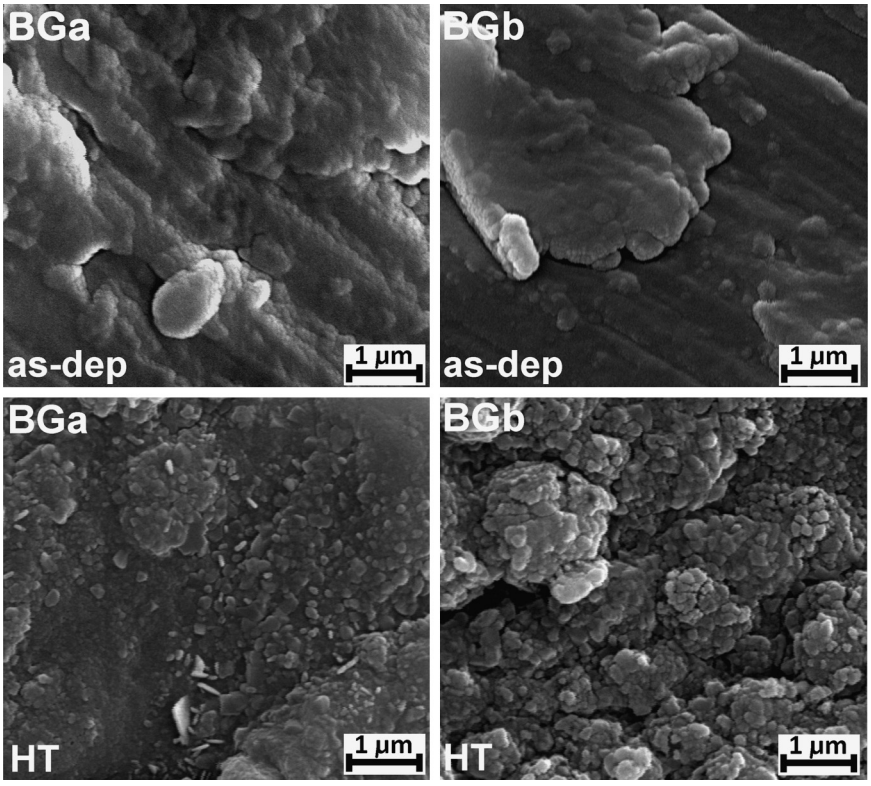

Fig. 2. SEM micrographs for the BG/Ti samples before and after heat-treatment at 750 °C for 2 h in air.

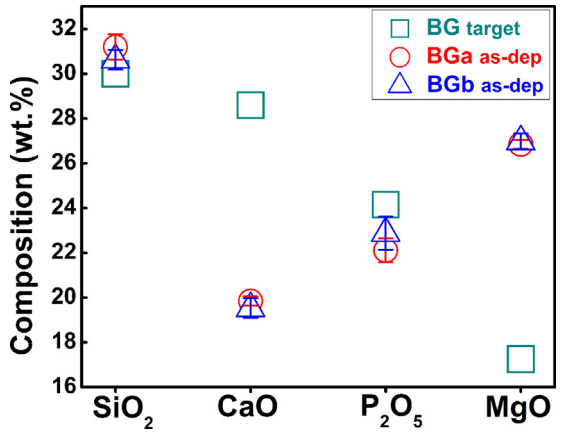

Fig. 3. Chemical oxide composition in wt.% for the BG target powder and for the BG/Ti as-deposited films. The values were calculated on the basis of EDX results. The data are represented as mean ± standard deviation ($n = 5$).

the dominant role here. As a matter of fact, the preferential sputtering of the lightest elements and the slower diffusing of heavier elements are well-accepted phenomena [18].

The compositional differences determined by the D_{T-S} variation were not statistically significant ($p > 0.05$). The result is logical, as both target-to-substrate distances used in this study are shorter than the mean free paths of atoms under the deposition conditions used.

3.4. XRD results

The XRD patterns recorded in symmetric geometry for the target powder, BG films heat-treated at 750 °C for 2 h in air, and bare Ti substrates annealed under identical conditions are compared in Fig. 4. The target powder is amorphous within the experimental sensitivity limit showing a pronounced hump centered at $2\theta \approx 30°$ (Fig. 4a), typical to amorphous bioglass structure [24,26]. The most intense peaks in the XRD patterns of the films correspond to the Ti substrate (ICDD: 03-44-1294). The intensity scales of the graphical representations were therefore chosen to emphasize the lower intensity lines originating from the films. As expected from a low temperature deposition process under non-equilibrium conditions [26], both as-deposited BG films were amorphous (data not shown). Upon the PDHT two well-defined crystalline oxide phases (TiO_2-rutile, $MgSiO_3$) and three titanium silicide-type compounds (TiSi, Ti_5Si_4 and Ti_5Si_3) were formed, suggesting the occurrence of strong atomic inter-diffusion phenomena through the BG–Ti interface. For the inter-metallic phases, slight shifts relative to the ICDD reference files were noticed in 2θ diffraction angles and intensity ratio, which are probably caused by: (i) their ill-defined stoichiometry derived from elemental gradient concentrations, leading to lattice distortions and (ii) the superposition of the XRD

Table 1
Standard free energy values of the oxidation reactions [33] and the atomic weights of the elements present in the target bioglass formulation.

	Chemical element			
	Si	Ca	P	Mg
Oxides' Gibbs energy of formation (kJ mol^{-1}) $T = 350$ °C	−1016.5 (SiO_2)	−1139.1 (CaO)	−1215.3 (P_2O_5)	−1035.7 (MgO)
Atomic weight (a.u.)	27.977	39.962	30.974	24.305

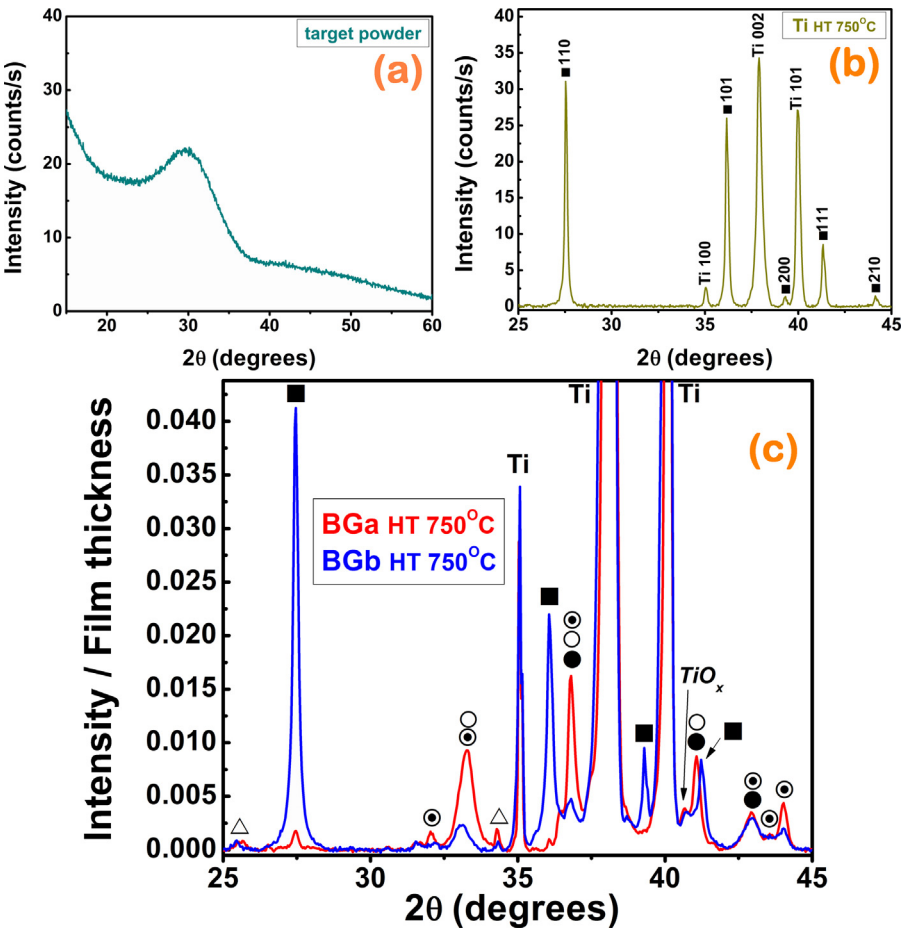

Fig. 4. XRD patterns recorded in symmetric geometry (θ–θ) for: (a) the BG target powder; (b) the heat-treated Ti bare substrate; and (c) the heat-treated BGa and BGb films. (■ = TiO_2 (rutile) – ICDD: 01-089-4920; ● = Ti_5Si_3 – ICDD: 00-029-1362; ⊙ = Ti_5Si_4 – ICDD: 00-027-0907; ○ = TiSi – ICDD: 00-017-0424; △ = $MgSiO_3$–ICDD: 01-075-1627).

peaks of Ti_xSi_y-type phases, which impedes an accurate association of the lines to each type of Ti_xSi_y phase.

Higher contents of Ti_xSi_y-type phases coexist with lower contents of rutile in BGa films (shorter D_{T-S}), contrarily to what can be observed for BGb films (longer D_{T-S}) in which the phase ratio was reversed. Several weak lines likely associated to small amounts of titanium sub-oxide phases (Ti_6O_{11} or Ti_4O_7) were also identified, whose formation could be due to some incomplete oxidation reactions which took place at titanium substrate surface during the PDHT. The occurrence of magnesium silicate-like phases at 750 °C, a temperature lower than the crystallization temperatures revealed by DTA for the starting BG powder, could be caused by the Mg enrichment observed in the sputtered films.

3.5. FTIR measurements

Fig. 5 shows the infrared absorption spectra of the BG target, as-deposited and PDHT BGa and BGb films. All spectra exhibit a broad prominent absorption band with two intensity maxima within the range of 800–1100 cm^{-1}, which is the IR fingerprint of silica-based glasses. Structural Q^n_{Si} species with low n values are expected in BG target and in the as-deposited films from their amorphous character (Fig. 4a), low silica contents coupled with relatively high concentrations of network modifiers (Fig. 3) [34]. The higher intensity maxima of the IR envelope observed for BG target could be attributed to a juxtaposition of the asymmetric stretch vibrations of Si—O^- bonds in Q^3 and Q^2 tetrahedral units (1005 cm^{-1}), and in Q^2 and Q^1 tetrahedral units (940 cm^{-1}). The weaker shoulders centered at 856 and 564 cm^{-1} might correspond to the Si—O^- bonds in Q^1 and Q^0 tetrahedral units, and to the Si—O—Si rocking motions, respectively [34,35].

As the BG target and films contain significant amounts of P_2O_5 (Fig. 3), the vibration effects of the Q^n_P species, which cover the 400–1400 cm^{-1} region of FTIR spectra, cannot be neglected [35], which might be also superimposed to the more intense vibration bands of Q^n_{Si} species.

The small differences observed in the FTIR spectra of the as-deposited films relative to the BG target spectrum in terms of shape and positions of the bands derived from the non-stoichiometric target-to-substrate transfer and the consequent glass network rearrangements occurring upon film growth [17,26]. CaO and MgO are generally viewed as glass network modifiers. However, it had been recently demonstrated that MgO possesses a double structural role in glass: (i) network modifier (disrupting the silicate network by creating non-bridging oxygen atoms) and (ii) entering the silicate network as tetrahedral "MgO_4" species [36,37].

The "MgO_4" species require charge balancing by cations (in our case: Ca^{2+}) and, therefore, the number of available modifier cations will be reduced, resulting in a more polymerized glass network [36,37]. This might explain the enhanced intensities of the band corresponding to structural species with more bridging oxygen atoms (Q^3 and Q^2 units) relative to the band corresponding to Q^2 and Q^1 units in the as-deposited films. Band shifts and modifications in their intensity ratios occurred between BGa and BGb films having a similar composition (Fig. 3). These structural changes were solely induced by the D_{T-S} variations that interfere with the physical magnetron sputtering process (number of atoms arriving at the substrate, ad-atoms energy) [18,28,29]. Similar observations have

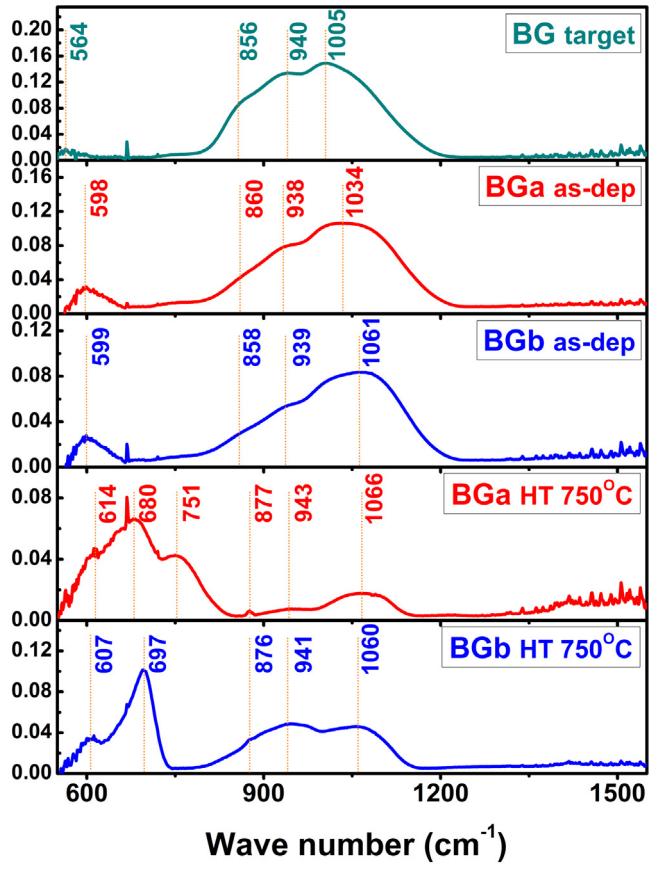

Fig. 5. FTIR spectra recorded in ATR mode for the BG target powder and for the as-deposited and heat-treated BGa and BGb films.

been reported for bioglass films deposited by PLD by Liste et al. [16], who underlined that short range structural differences could be detected by FTIR even when the target stoichiometry was nearly congruently transferred to the PLD coatings.

Dramatic modifications occurred in the IR spectra envelope for both films upon PDHT, including a significant intensity decrease of the 800–1100 cm^{-1} bands, and the appearance of new vibrational modes at 680 cm^{-1} (BGa), 697 cm^{-1} (BGb), 751 cm^{-1} (BGa) and ~876 cm^{-1} (BGa and BGb). Their causality will be discussed later.

3.6. Pull-out testing

Selecting the experimental coating conditions leading to enhanced bonding strength is of paramount importance when designing bio-functional coated medical devices. According to international standards, only pull-out adherence values higher than ~51 MPa are acceptable for these BG/Ti implant coatings [38,39]. This means that the selected epoxy adhesive with a bonding limit of ~85 MPa is strong enough to evaluate the suitability of the coatings' adherence. The glue bonding strength tested independently on bare titanium plates revealed that failure always occurred in the glue's volume at 80–85 MPa, thus confirming its technical specification, with glue traces felt in the detached areas. In case of BG/Ti couples, failure systematically occurred at the BG/Ti interface with the BG film being always cleanly detached from the Ti substrate. For the as-deposited films, rather low adhesion values have been recorded: 38.2 ± 3.0 MPa (BGa) and 31.5 ± 4.0 MPa (BGb). The two tailed t testing (assuming unequal variances) revealed statistically significant differences ($p \approx 0.032$) between these adherence values, which compare well with those reported by Mardare et al. [8] for sputtered films deposited from a BG target with the same chemical formulation.

The PDHT given to the BG/Ti couples in the present work was aimed at releasing the internal stresses in the sputtered BG films to enhance the pull-out tensile strength. The measured adherence values of 60.3 ± 4.6 MPa (BGa) and 39.4 ± 4.1 MPa (BGb) are statistically highly significant ($p \approx 0.00002$). The bonding strength value recorded for BGa films being higher than that required by mandatory international standards [38,39]. Since the PDHT films show some sub-micron sized inter-granular cavities or porosity, the possibility for the glue to go through and directly bond to Ti substrate, thus enhancing the bonding strength, cannot be completely discarded. But the importance of this factor might be neglected because the glue's high viscosity and tendency to rapidly harden upon thermal curing oppose to its penetration in the sub-micron porosity. The absence of glue traces in the detached areas analyzed by SEM also supports this hypothesis, making the recorded bonding strength values very promising. Moreover, it is reasonable to accept that cohesion strength (tendency of identical molecules to stick to each another) within the BG film and Ti_xSi_y inter-diffusion layer is higher than the recorded values of interfacial adhesion.

4. Discussion

The attempts made so far to combine the good mechanical properties of implants with the bioactive surfaces conferred by BG have been mitigated by low bonding strength of the joined materials, limiting their further exploitation for medical practice [2,5]. A low porosity of the film and its strong bond to the metallic substrate are also prerequisites for a hermetic (halting the substrate metallic ions' diffusion into surrounding living tissue) implant-type coating. These drawbacks justify the pertinence of this work.

The similarity between the adhesion values measured for the as-sputtered films and those reported for similar structures by Mardare et al. [8] was noticed. These authors also performed PDHT but at a much higher temperatures (900–1000 °C) and observed a significant declining in the films' adherence. This is not surprising considering that titanium undergoes an allotropic phase transformation at 882 °C, from a low temperature hexagonal close-packed α-Ti phase to a high temperature body-centered cubic β-Ti phase, which is accompanied by a decrease in volume [40]. This volume change derives from the enhanced electronic repulsion between the most adjacent neighboring atoms, 12 in case of α-Ti, compared to 8 in β-Ti, consequently leading to a decrease of the inter-atomic distances [41]. The significant stresses generated during this transformation lead to poor mechanical adherence and even delamination of the coating BG layer.

These assumptions, together with our desire for minimizing the crystallization of BG films and its negative impact on bioactivity [42–44], led us selecting a lower PDHT temperature. The intent was inducing Ti–BG inter-diffusion and smoothing their abrupt interface, while using low heating and cooling rates (5 °C min^{-1}) to minimize the interfacial stresses at the end of the thermal cycle.

The higher bonding strength values obtained for the PDHT BGa films (60.3 ± 4.6 MPa) deposited at the shorter D_{T-S} are in good agreement with the hypothesized higher contents of Ti_xSi_y phases detected for BGa structures (Fig. 4c). The significant decrease in intensity of the original BG vibration bands, and the appearance of new ones in the lower wave numbers range (550–800 cm^{-1}) registered after PDHT (Fig. 5) show that FTIR analysis also support these XRD findings. These changes are attributed to the inter-metallic Ti_xSi_y phases' formation and the concomitant occurrence of oxidation reactions.

The IR band integral area can roughly be expressed as a product of the absorption coefficient in the region of stretching vibrations (800–1100 cm^{-1}) and the number of Q_{Si}^n and Q_P^n species which absorb the infrared light. Therefore, the integral area of these bands could be regarded as an indicator of the BG layer's mass,

proportional to the film's thickness. The gradual consume of BG film with the formation of Ti_xSi_y-type phases leads to a concomitant decreasing intensity of the Q^n_{Si} IR dominant bands. These changes are more pronounced for BGa structures, being in good agreement with the XRD results. The more extended inter-diffusion process is also consistent with the higher bonding strength values measured by pull-out tests.

The random thermal motion at temperatures above T_g enables atomic rearrangements such as diffusion/sintering. On the other hand, the high affinity of Ti atoms toward oxygen and the hindered direct contact of the Ti substrate with oxygen from the air atmosphere, is likely leading to the breakage of Si—O bonds and to the formation of Ti_xSi_y compounds [13,45]. This makes the vibration bands of Q^n_{Si} species less predominant, enabling the superimposed vibration modes of Q^n_P species to become visible. Thereby, the vibration bands corresponding to the asymmetric stretching (ν_3) of PO_4^{3-} groups (1066 cm^{-1}), HPO_4^{2-} band (877 cm^{-1}), stretching of P—O—P bridges (751 cm^{-1}) were identified in the PDHT BGa (Fig. 5) [34,35,46]. The hydrogen phosphate band could be generated by the outspoken glass hygroscopic character; the possibility for water molecules to interact with phosphate groups during the PDHT cannot be excluded. Also, the contributions of the symmetric stretching (ν_1) of PO_4^{3-} groups (~962 cm^{-1}) [46], Ti—O—Si bands (~960 cm^{-1}) [47] and bending mode (ν_4) of PO_4^{3-} groups (~600 cm^{-1}) [46] could be taken into account.

Similar structural alterations could be noticed for PDHT BGb structures, but in a lesser extent. A new band centered is observed for BGb coatings at ~697 cm^{-1}, while appears with a lower intensity and slightly shifted to lower wave numbers (~680 cm^{-1}) in the case of BGa samples. This band ascribed to the TiO_2 vibrations [48,49], correlates well with the rutile evolution in the heat-treated BG films as depicted by XRD (Fig. 4). The structural differences between the PDHT BGa and PDHT BGb coatings are due to the cosine-like angular distribution of sputtered atoms. The consequent decrease of atomic flux impinging the substrate with increasing D_{T-S} is likely to affect the growing film's properties such as density, compactness, columnar structure, and adhesion.

The more abundant and energetic species arriving at the growing film's surface for the shorter D_{T-S} (as demonstrated by the higher deposition rate) will enhance density of the resulting BG film. The ad-atoms with higher kinetic energy will be able to rearrange in conditions closer to their thermal equilibrium. An additional rationale should be considered, the deposition temperature is dependent on the intensity of substrate bombardment. The Thornton model [50] states that more compact and dense films can be prepared with increasing substrate temperature operating at low sputtering pressure. Therefore, the decrease of the D_{T-S} will increase the particle bombardment leading to higher mobility of ad-atoms and an increase of substrate temperature, which in turn will determine the film densification (compactness), with less voids and inhomogeneities in its structure [51]. These processes could have an important role on the amorphous matrix rearrangement, as the energetic bombardment could induce bond distortions and/or displacement of atoms from their equilibrium locations [52]. This could also account for the short-range order modification observed by FTIR for the two types of as-deposited films having quite similar compositions.

According to Saiz and Tomsia [13,53], the formation of Ti_xSi_y-like phases during the PDHT is due to the occurrence of the following two interfacial chemical reactions:

$$8Ti + 3SiO_2\ \{glass\} \rightarrow Ti_5Si_3 + 3TiO_2\ \{glass\} \quad (1)$$

$$5Ti + 3SiO_2 \rightarrow Ti_5Si_3 + 3O_2\uparrow . \quad (2)$$

The formation of a 150 nm Ti_5Si_3 interfacial layer with good lattice matching with the Ti substrate and strain relaxation provided by the nanostructured interface was pointed out as the main factor responsible for the strong bond between the silicide layer and the Ti substrate, without negatively affecting the bioactivity/biocompatibility [12,13]. Moreover, the thermal expansion coefficient of the Ti_5Si_3 inter-metallic compound up to 1000 °C is of ~9.1×10^{-6} C^{-1}, thus similar to that of pure titanium [54].

According to Saiz et al. [12,13,53], enhanced film adherence is favored by the reaction (1), as the liberation of oxygen from reaction (2) would eventually result in the formation of bubbles and an opposite effect on the interfacial adhesion strength. The presence of TiO_2 in our BG samples and the longer heat-treatment time (which disables the possible ebullience of oxygen) also suggests reaction (1) as the most likely chemical for inter-diffusion route.

For compact films, deformation/flow at temperatures above T_g could culminate with an excellent sealing of the glass/Ti interface, hindering the direct contact with the air atmosphere, allowing the Si atoms reacting with the substrate and partly refraining the Ti oxidation. Ti can be easily oxidized in air above 120 °C, with strong oxidation effects being induced with increasing annealing temperatures [30,55]. In this work a bare titanium substrate was used as control sample, and heat-treated under the same conditions as sputtered films. The XRD analysis of such a sample indicated massive surface oxidation with the formation of pure rutile phase at the end of the thermal cycle (Fig. 4b). Therefore, to avoid excessive oxidation, the Ti substrate should not come into direct contact with free oxygen during the thermal-treatment. Besides, earlier experimental findings [56] suggested that a silicon-rich environment could partly inhibit the metal from oxidation. Our results obtained for the less compact BGb films also support this hypothesis. Oxygen diffusion and the consequent formation of rutile would concomitantly occur with the formation of Ti_xSi_y phases at the surface of the Ti substrate. Interestingly, even in this situation BGb films' adhesion is not diminished, but slightly increased ($p \approx 0.008$). We hypothesize that the contact of Ti with oxygen atoms from the glass might allow atomic diffusion, enhancing the chemical interfacial bonding strength. On the other hand, the more open structure BGb films facilitates the diffusion of oxygen from atmosphere through the films and the direct oxidation of the Ti substrate forms rutile crystals, which might provide some mechanical interlocking likely contributing to bonding strength enhancement [57]. Thereby, our results also suggest that the interfacial titanium silicide layer lowers the driving force for TiO_2 formation and crystallization (BGa), but if the films are less compact, this kinetic trend is counterbalanced by the free oxygen diffusion from the surrounding atmosphere, which enhances the substrate oxidation (BGb).

The Ti silicidation reaction occurs when its surface is brought in intimate contact with the silicon-rich glassy matrix, and the heat treatment temperature is high enough to promote the inter-diffusion [58]. Si is the dominant diffusion specie in this reaction, as Ti is known to be one of the slowest diffusing transition metals in silicon [59]. The temperature for the transport of Si in silicides is above 550 °C [60]. Some authors consider that the diffusion of Si into Ti proceeds first at the boundary of Ti grains and then, with the raising of temperature, within the grains. The inter-diffusion process occurs before the formation of any crystalline phase [58,59].

The Ti_xSi_y nucleation could be extra-stimulated by the presence of an intermixing Ti–Si layer resulting from ballistic implantation of Si atoms in the first atomic layers of the substrate during the RF-MS deposition process [58], which will initiate the growth of the Ti_xSi_y crystalline phases with increasing temperature, obeying a diffusion-controlled growth law.

Multiple factors that might have determined the preferential formation of the different compounds identified in the BGa and BGb systems include: Gibbs free energy of the compounds, enthalpy of reaction, activation energy, reaction rate constant at the PDHT temperature, *etc.* Guan et al. [61] proposed the following sequence for

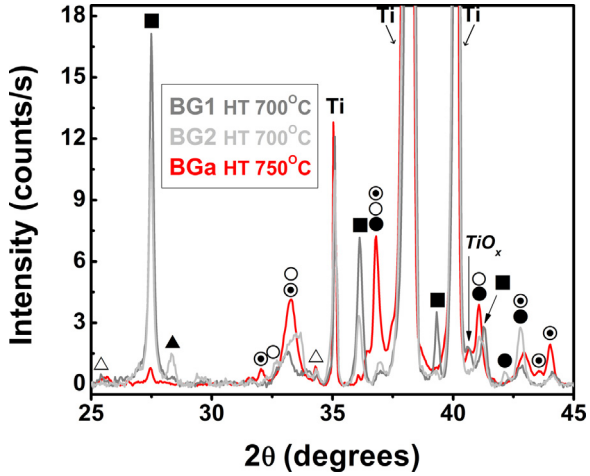

Fig. 6. XRD patterns recorded in symmetric geometry (θ–θ) for the BGa, BG1 and BG2 heat-treated films. (■ = TiO_2 (rutile) – ICDD: 01-089-4920; ● = Ti_5Si_3 – ICDD: 00-029-1362; ⊙ = Ti_5Si_4 – ICDD: 00-027-0907; ◯ = TiSi – ICDD: 00-017-0424; △ = $MgSiO_3$ – ICDD: 01-075-1627; ▲ = $Mg_2(SiO_3)_2$ (enstatite) – ICDD: 01-86-0430).

the entropies of formation of titanium silicides: Ti_5Si_3 < Ti_5Si_4 < TiSi, meaning the reverse order (Ti_5Si_3 > Ti_5Si_4 > TiSi) in terms of thermodynamic stability. These transformations are dependent on reaction time and temperature. If the temperature is high enough to enable Ti_5Si_3 formation, and sufficient time will pass, all titanium silicide forms will be converted into Ti_5Si_3 with TiO_2 as second phase. The relative amount of TiO_2 will increase if oxygen atoms can diffuse from the atmosphere through the bioglass film to directly oxidize the Ti substrate (BGb). At the beginning, the interface consists of 100 at.% Ti atoms (substrate) and only ~30 at.% Si atoms (glass). This atomic ratio favors the formation of Ti_5Si_3 rather than TiSi or Ti_5Si_4. Therefore, the presence of TiSi and Ti_5Si_4 in the heat-treated films can be regarded as intermediate phases as a consequence of the insufficient reaction time. The simultaneous growth of TiSi, Ti_5Si_4 and Ti_5Si_3 is not unprecedented [62,63]. The scientific literature offers many contradictions regarding the activation energies and the reaction rate constants for the formation of titanium silicides' formation, hampering an accurate estimation of their relative amounts.

The good interfacial BG/Ti bonding achieved for the RF-MS coatings upon PDHT appears as a potential algorithm for broadening the biomedical applications of BG/Ti implants. But could this proposed algorithm also work for other BG compositional systems? In order to ascertain this, two other glass compositions, BG1 (wt.%): SiO_2 – 40.08, CaO – 29.1, MgO – 8.96, P_2O_5 – 6.32, CaF_2 – 5.79, B_2O_3 – 5.16, and Na_2O – 4.59, having T_g = 580 °C [34] and BG2 (wt.%): SiO_2 – 46.06, CaO – 28.66, MgO – 8.83, P_2O_5 – 6.22, CaF_2 – 5.7, and Na_2O – 4.53, with T_g = 600 °C [64], have been sputtered under the same conditions as BGa, followed by a PDHT at 700 °C for 2 h. The XRD patterns presented in Fig. 6 show that similar reaction processes were induced at their BG/Ti interfaces, demonstrating the repeatability of the procedure. These findings are likely encouraging further studies aiming at disclosing the detailed effects of relevant process variables such as sputtering conditions, heat treatment temperature *versus* T_g, the intrinsic viscosity of the glass, film compactness, and so on.

5. Conclusions

The study of the effects of target-to-substrate distance and post-deposition heat treatment (PDHT) on the compositional, structural and adherence properties of RF-MS BG films deposited onto Ti substrates enable the following conclusions to be drawn:

1. The bioglass composition is not stoichiometrically transferred to the substrate; the deposited films become enriched in the lighter elements and depleted in the heavier ones. Increasing the target-to-substrate distance favors lower compactness/higher oxygen permeability;
2. A PDHT temperature of 750 °C > T_g (716 °C) provided the necessary energy for the inter-diffusion phenomena to occur at the BG/Ti interface with the formation of inter-metallic (TiSi, Ti_5Si_4, Ti_5Si_3) compounds that greatly enhanced the interfacial bonding strength by ~57% for the most impervious BGa (D_{T-S} = 35 mm), and by ~25% for the most oxygen permeable BGb films (D_{T-S} = 55 mm). The higher oxygen permeability of BGb films led to a more extensive formation of TiO_2 upon post-deposition heat-treatment;
3. Similar inter-diffusion events were induced by applying the same technological approach to other bioglass formulations. The strong adherence values measured for the PDHT BG/Ti couples, which are higher than those imposed by international standards, make the proposed technological algorithm very promising for the development of high performance oral and orthopedic bioglass coated implants.

Acknowledgments

G.E.S. and A.C.P. are thankful for the financial support from the Romanian National Authority for Scientific Research through the UEFISCDI TE 49/05.10.2011 (TE-0164). The support from CICECO is also acknowledged.

References

[1] L.L. Hench, The story of Bioglass®, Journal of Materials Science Materials in Medicine 17 (2006) 967–978.
[2] J.R. Jones, A. Clare, Bio-Glasses: An Introduction, 1st ed., John Wiley & Sons Ltd, 2012.
[3] J.A. Epinette, M.T. Manley, R.G.T. Geesink, Fifteen Years of Clinical Experience with Hydroxyapatite Coatings in Joint Arthroplasty, 1st ed., Springer-Verlag, Paris, 2003.
[4] A. Hoppe, N.S. Güldal, A.R. Boccaccini, A review of the biological response to ionic dissolution products from bioactive glasses and glass-ceramics, Biomaterials 32 (2011) 2757–2774.
[5] A. Sola, D. Bellucci, V. Cannillo, A. Cattini, Bioactive glass coatings: a review, Surface Engineering 27 (2011) 560–572.
[6] G. Goller, The effect of bond coat on mechanical properties of plasma sprayed bioglass–titanium coatings, Ceramics International 30 (2004) 351–355.
[7] L. Peddi, R.K. Brow, R.F. Brown, Bioactive borate glass coatings for titanium alloys, Journal of Materials Science Materials in Medicine 19 (2008) 3145–3152.
[8] C.C. Mardare, A.I. Mardare, J.R.F. Fernandes, E. Joannia, S.C.A. Pina, M.H.V. Fernandes, R.N. Correia, Deposition of bioactive glass-ceramic thin-films by RF magnetron sputtering, Journal of the European Ceramic Society 23 (2003) 1027–1030.
[9] R.A. Surmenev, A review of plasma-assisted methods for calcium phosphate based coatings fabrication, Surface and Coatings Technology 206 (2012) 2035–2056.
[10] Q. Fu, E. Saiz, M.N. Rahaman, A.P. Tomsia, Bioactive glass scaffolds for bone tissue engineering: state of the art and future perspectives, Materials Science and Engineering C 31 (2011) 1245–1256.
[11] A.R. Boccaccini, S. Keim, R. Ma, Y. Li, I. Zhitomirsky, Electrophoretic deposition of biomaterials, Journal of the Royal Society Interface 7 (2010) S581–S613.
[12] S. Lopez-Esteban, C.F. Gutierrez-Gonzalez, L. Gremillard, E. Saiz, A.P. Tomsia, Interfaces in graded coatings on titanium-based implants, Journal of the Biomedical Materials Research, Part A 88A (2009) 1010–1021.
[13] J.M. Gomez-Vega, E. Saiz, A.P. Tomsia, T. Oku, K. Suganuma, G.W. Marshall, S.J. Marshall, Novel bioactive functionally graded coatings on Ti6Al4V, Advanced Materials 12 (2000) 894–898.
[14] L. Altomare, D. Bellucci, G. Bolelli, B. Bonferroni, V. Cannillo, L. De Nardo, R. Gadow, A. Killinger, L. Lusvarghi, A. Sola, N. Stiegler, Journal of Materials Science Materials in Medicine 22 (2011) 1303–1319.
[15] A. Cattini, L. Łatka, D. Bellucci, G. Bolelli, A. Sola, L. Lusvarghi, L. Pawłowski, V. Cannillo, Surface and Coatings Technology 220 (2013) 52–59.
[16] S. Liste, P. González, J. Serra, J.P. Borrajo, S. Chiussi, B. León, M. Pérez-Amor, J. García López, F.J. Ferrer, Y. Morilla, M.A. Respaldiza, Study of the stoichiometry transfer in pulsed laser deposition of bioactive silica-based glasses, Thin Solid Films 453–454 (2004) 219–223.
[17] G.E. Stan, I. Pasuk, M.A. Husanu, I. Enculescu, S. Pina, A.F. Lemos, D.U. Tulyaganov, El Mabrouk Fs K., J.M.F. Ferreira, Highly adherent bioactive glass

thin films synthetized by magnetron sputtering at low temperature, Journal of Materials Science Materials in Medicine 22 (2011) 2693–2710.
[18] K. Wasa, M. Haber, H. Adachi, Thin Film Materials Technology: Sputtering of Compound Materials, 1st ed., William Andrew, New York, 2005.
[19] A. Balamurugan, G. Balossier, J. Michel, J.M.F. Ferreira, Electrochemical and structural evaluation of functionally graded bioglass–apatite composites electrophoretically deposited onto Ti6Al4V alloy, Electrochimica Acta 54 (2009) 1192–1198.
[20] G.E. Stan, A.C. Popescu, I.N. Mihailescu, D.A. Marcov, R.C. Mustata, L.E. Sima, S.M. Petrescu, A. Ianculescu, R. Trusca, C.O. Morosanu, On the bioactivity of adherent bioglass thin films synthesized by magnetron sputtering techniques, Thin Solid Films 518 (2010) 5955–5964.
[21] L. Floroian, F. Sima, M. Florescu, M. Badea, A.C. Popescu, N. Serban, I.N. Mihailescu, Double layered nanostructured composite coatings with bioactive silicate glass and polymethylmetacrylate for biomimetic implant applications, Journal of Electroanalytical Chemistry 648 (2010) 111–118.
[22] J. Zhang, C. Jia, Z. Jia, J. Ladegard, Y. Gu, J. Nie, Strengthening mechanisms in carbon nanotube reinforced bioglass composites, Frontiers of Chemical Science and Engineering 6 (2012) 126–131.
[23] D. Bellucci, V. Cannillo, A. Sola, Coefficient of thermal expansion of bioactive glasses: available literature data and analytical equation estimates, Ceramics International 37 (2011) 2963–2972.
[24] A. Goel, S. Kapoor, R.R. Rajagopal, M.J. Pascual, H.W. Kim, J.M.F. Ferreira, Alkali-free bioactive glasses for bone tissue engineering: a preliminary investigation, Acta Biomaterialia 8 (2012) 361–372.
[25] J.M. Oliveira, R.N. Correia, M.H. Fernandes, Surface modifications of a glass and a glass–ceramic of the $MgO–3CaO·P_2O_5–SiO_2$ system in a simulated body fluid, Biomaterials 16 (1995) 849–854.
[26] C. Berbecaru, G.E. Stan, S. Pina, D.U. Tulyaganov, J.M.F. Ferreira, The bioactivity mechanism of magnetron sputtered bioglass thin films, Applied Surface Science 258 (2012) 9840–9848.
[27] A.C. Galca, V. Stancu, M.A. Husanu, C. Dragoi, N.G. Gheorghe, L. Trupina, M. Enculescu, E. Vasile, Substrate–target distance dependence of structural and optical properties in case of $Pb(Zr,Ti)O_3$ films obtained by pulsed laser deposition, Applied Surface Science 257 (14) (2011) 5938–5943.
[28] A. Palmero, H. Rudolph, H.P.M. Habraken, One-dimensional analysis of the rate of plasma-assisted sputter deposition, Journal of Applied Physics 101 (2007), 083307–083307-6.
[29] E.D. van Hattum, A. Palmero, W.M. Arnoldbik, H. Rudolph, F.H.P.M. Habraken, On the ion and neutral atom bombardment of the growth surface in magnetron plasma sputter deposition, Applied Physics Letters 91 (2007), 171501–171501-3.
[30] G.E. Stan, Adherent functional graded hydroxylapatite coatings produced by sputtering deposition techniques, Journal of Optoelectronics and Advanced Materials 11 (2009) 1132–1138.
[31] I. Mercioniu, S. Ciuca, I. Pasuk, A. Slav, C. Morosanu, M. Bercu, Thickness dependence of crystallization process for hydroxyapatite thin films, Journal of Optoelectronics and Advanced Materials 9 (2007) 2535–2538.
[32] K. Anselme, M. Bigerelle, Topography effects of pure titanium substrates on human osteoblast long-term adhesion, Acta Biomaterialia 1 (2005) 211–222.
[33] C.B. Alcock, Thermochemical Processes—Principles and Models, 1st ed., Butterworth-Heinemann, Oxford, 2001.
[34] S. Agathopoulos, D.U. Tulyaganov, J.M.G. Ventura, S. Kannan, M.A. Karakassides, J.M.F. Ferreira, Formation of hydroxyapatite onto glasses of the $CaO–MgO–SiO_2$ system with B_2O_3, Na_2O CaF_2 and P_2O_5 additives, Biomaterials 27 (2006) 1832–1840.
[35] G. Socrates, Infrared and Raman Characteristic Group Frequencies—Tables and Charts, 1st ed., John Wiley & Sons Ltd., 2007.
[36] S.J. Watts, M.D. O'Donnell, R.V. Law, R.G. Hill, Influence of magnesia on the structure and properties of bioactive glasses, Journal of Non-Crystalline Solids 256 (2010) 517–524.
[37] R.G. Hill, D.S. Brauer, Predicting the glass transition temperature of bioactive glasses from their molecular chemical composition, Acta Biomaterialia 7 (2011) 3601–3605.
[38] ISO 13779-2, Implants for Surgery—Hydroxyapatite—Part 2: Coatings of Hydroxyapatite, 2008 http://www.iso.org/iso/iso_catalogue/catalogue_tc/catalogue_detail.htm?csnumber=43827
[39] Food and Drug Administration [FDA], Calcium Phosphate (Ca-P) Coating Draft Guidance for Preparation of FDA Submissions for Orthopedic and Dental Endooseous Implants, 1997, pp. 1–14.
[40] I.W. Donald, P.M. Mallinson, B.L. Metcalfe, L.A. Gerrard, J.A. Fernie, Recent developments in the preparation, characterization and applications of glass- and glass–ceramic-to-metal seals and coatings, Journal of Materials Science 46 (2011) 1975–2000.
[41] W. Hume-Rothery, R.E. Smallman, C.W. Haworth, Structure of Metals and Alloys, 1st ed., The Metal and Metallurgical Trust, London, 1969.
[42] P. Li, Q. Yang, F. Zhang, T. Kokubo, The effect of residual glassy phase in a bioactive glass–ceramic on the formation of its surface apatite layer in vitro, Journal of Materials Science Materials in Medicine 3 (1992) 452–456.
[43] O. Peitl Filho, G.P. LaTorre, L.L. Hench, Effect of crystallization on apatite-layer formation of bioactive glass 45S5, Journal of Biomedical Materials Research 30 (1996) 509–514.
[44] A. Sola, D. Bellucci, M.G. Raucci, S. Zeppetelli, L. Ambrosio, V. Cannillo, Heat treatment of $Na_2O–CaO–P_2O_5–SiO_2$ bioactive glasses: densification processes and postsintering bioactivity, Journal of Biomedical Materials Research A 100A (2012) 305–322.
[45] A. Pazo, E. Saiz, A.P. Tomsia, Silicate glass coatings on Ti-based implants, Acta Materialia 46 (1998) 2551–2558.
[46] M. Markovic, B.O. Fowler, M.S. Tung, Preparation and comprehensive characterization of a calcium hydroxyapatite reference material, Journal of Research of the National Institute of Standards and Technology 109 (2004) 553–568.
[47] E. Pabón, J. Retuert, R. Quijada, A. Zarate, $TiO_2–SiO_2$ mixed oxides prepared by a combined sol–gel and polymer inclusion method, Microporous and Mesoporous Materials 67 (2004) 195–203.
[48] Y. Gao, Y. Masuda, W.-S. Seo, H. Ohta, K. Koumoto, TiO_2 nanoparticles prepared using an aqueous peroxotitanate solution, Ceramics International 30 (2004) 1365–1368.
[49] Y. Han, H.-S. Kim, H. Kim, Relationship between synthesis conditions and photocatalytic activity of nanocrystalline TiO_2, Journal of Nanomaterials (2012), http://dx.doi.org/10.1155/2012/427453, Article ID 427453 (10p).
[50] J. Thornton, The microstructure of sputter-deposited coatings, Journal of Vacuum Science and Technology A 4 (1986) 3059–3065.
[51] G.F. Iriarte, J.G. Rodriguez, F. Calle, Effect of substrate–target distance and sputtering pressure in the synthesis of AlN thin films, Microsystem Technologies 7 (2011) 1381–1386.
[52] S. Zhang, D. Sun, Y. Fu, H. Du, Q. Zhang, Effect of sputtering target power density on topography and residual stress during growth of nanocomposite nc-TiN/a-SiN_x thin films, Diamond & Related Materials 13 (2004) 1777–1784.
[53] E. Saiz, A.P. Tomsia, J.M. Gomez-Vega, S. Fujino, Graded coatings for metallic implant alloys, in: C.A. Lewinsohn, M. Singh, R. Loehman (Eds.), Advances in Joining of Ceramics, 138, John Wiley & Sons Ltd., 2012, pp. 159–172.
[54] G. Frommeyer, R. Rosenkranz, in: O.N. Senkov, D.B. Miracle, S.A. Firstov (Eds.), Metallic Materials with High Structural Efficiency, 1st ed., Springer, 2004, pp. 287–308.
[55] S. Mohammadi, L. Wictorin, L.E. Ericson, P. Thomsen, Cast titanium as implant material, Journal of Materials Science Materials in Medicine 6 (1995) 435–444.
[56] C. Nobili, F. Nava, G. Ottaviani, M. Costato, G. De Santi, G. Queirolo, Titanium silicide formation in presence of oxygen, Active and Passive Electronic Components 15 (1992) 9–26.
[57] G.E. Stan, C.O. Morosanu, D.A. Marcov, I. Pasuk, F. Miculescu, G. Reumont, Effect of annealing upon the structure and adhesion properties of sputtered bio-glass/titanium coatings, Applied Surface Science 255 (2009) 9132–9138.
[58] O. Chaix-Pluchery, B. Chenevier, I. Matko, J.P. Sénateur, F. La Via, Investigations of transient phase formation in Ti/Si thin film reaction, Journal of Applied Physics 96 (2004) 361, 8p.
[59] B. Chenevier, O. Chaix-Pluchery, P. Gergaud, O. Thomas, F. La Via, Thermal expansion and stress development in the first stages of silicidation in Ti/Si thin films, Journal of Applied Physics 94 (2003) 7083 (8p).
[60] L.S. Hung, J. Gyulai, J.W. Mayer, S.S. Lau, M. Nicolet, Kinetics of $TiSi_2$ formation by thin Ti films on Si, Journal of Applied Physics 54 (1983) 5076 (5p).
[61] Q.L. Guan, H.Y. Wang, S.L. Li, C. Liu, Q.C. Jiang, Microstructure characteristics of products in Ti–Si system via combustion synthesis reaction, Journal of Materials Science 44 (2009) 1902–1908.
[62] S.T. Lakshmikumar, A.C. Rastogi, The growth of titanium silicides in thin film Ti/Si structures, Journal of Vaccum Science and Technology B 7 (1989) 604 (5p).
[63] T.H. Yang, K.S. Chi, L.J. Chen, Formation of Ti silicide nanocrystals in the amorphous interlayers in ultrahigh-vacuum-deposited Ti thin films on (0 0 1) Si, Journal of Applied Physics 98 (2005) 034302 (6p).
[64] D.U. Tulyaganov, S. Agathopoulos, P. Valerio, A. Balamurugan, A. Saranti, M.A. Karakassides, J.M.F. Ferreira, Synthesis, bioactivity and preliminary biocompatibility studies of glasses in the system $CaO–MgO–SiO_2–Na_2O–P_2O_5–CaF_2$, Journal of Materials Science Materials in Medicine 22 (2011) 217–227.